communications biology

Article

https://doi.org/10.1038/s42003-025-07524-y

Piezo1 promotes vibration-induced vascular smooth muscle injury by regulating the NF-κB/p65 axis

Check for updates

Yingshan Zeng[1,2], Zhiquan Wu[1,2], Mengtian Xiong[1,2], Zhishan Liang[1,2], Ziyu Chen[1,2], Huimin Huang[1,2], Hongyu Yang[1,2] ✉ & Qingsong Chen[1,2] ✉

Vibration induced damage to the peripheral circulatory system is thought to be an early stage of hand-arm vibration syndrome (HAVS) caused by occupational exposure to hand-transmitted vibration (HTV). This study investigated the mechanisms underlying vibration-induced vascular injury, focusing on the role of Piezo1, a mechanosensitive channel, and its association with the NF-κB/p65 signaling pathway. We demonstrated that vibration exposure leads to Piezo1-mediated upregulation of angiogenic chemokines, including CCL2, CCL5, CXCL1, CXCL2, and CXCL10, through the NF-κB/p65 pathway. To mimic the effects of vibration, a rat vibration model and a cellular vibration model were used. Animal and cellular models showed that vibration-induced vascular dysfunction while increasing Piezo1 expression. Piezo1 knockdown or p65 inhibition attenuated these effects, suggesting a crucial role for the Piezo1-NF-κB/p65 axis in vascular dysfunction. Furthermore, chemokines were identified as potential biomarkers for early diagnosis of HAVS in occupationally exposed individuals. These results highlight Piezo1 and the NF-κB/p65 pathway as potential therapeutic targets for HAVS and underscore the need for further validation in human samples and exploration of additional signaling mechanisms involved in vibration-induced vascular injury.

Hand-arm vibration syndrome (HAVS) is a progressive disorder caused by occupational exposure to hand-transmitted vibration (HTV)[1]. HAVS symptoms include neurosensory deficits, vascular disease, and hand pain[2]. HAVS is a common occupational disease in cold regions[3,4]. The feature used for diagnosis is cold-induced whitening of the fingers, which is called "vibration white finger" (VWF)[5]. The diagnosis of HAVS relies heavily on the report of a VWF, which requires a cold temperature to stimulate the finger[6]. This a painful experience for the patient, and its diagnostic utility in the early stages of injury is minimal[7]. In recent years, studies have focused on serum biomarkers and their correlation with hand-arm vibration injury, but the specific mechanism by which HTV causes HAVS has rarely been reported[8–10]. Also, the prevention and treatment of HAVS are limited and insufficient. Therefore, further research into the HAVS pathogenesis and exploration of new treatment strategies are important for working populations.

In the rat model, as in humans, vibration at or near the resonant frequency leads to increased oxidative stress, inflammation, and changes in vascular morphology, gene expression, and physiological function[11]. Vibration causes varying degrees of damage to vascular tissues, with a significant increase in vacuolization of smooth muscle cells[12,13]. The differentiated state of vascular smooth muscle cells is distinguished by the presence of specific contractile proteins, various of ion channels, and cell surface receptors, among other features[14]. This suggests that smooth muscle cells may respond to vibration exposure through ion channels. Piezo1 is a novel mechanosensitive membrane channel protein component of mechanically force-activated cation channels[15]. Piezo1 can mediate the response in mechanosensitive Ca^{2+} influx in vascular smooth muscle cells[16]. Recent studies have shown that Piezo1 is involved in myocardial infarction[17], angiogenesis[18], and apoptosis[19] *via* Ca^{2+} influx, and that knockdown or pharmacological inactivation of Piezo1 can reverse these phenomena[20,21]. Piezo1 signaling is a potential therapeutic target for inflammation and the vascular system[22]. Thus, revealing the role of Piezo1 in vibration-induced vascular injury is critical for understanding the molecular mechanisms of HAVS and identifying therapeutic targets or early diagnostic markers for HAVS.

The nuclear factor-kappa B (NF-κB) family of transcription factors regulates various cellular responses[23]. However, aberrant activation of

[1]Department of Occupational and Environmental Health, School of Public Health, Guangdong Pharmaceutical University, Guangzhou, China. [2]Guangdong Provincial Engineering Research Center of Public Health Detection and Assessment (2019GCZX012), Guangdong Pharmaceutical University, Guangdong, China. ✉e-mail: gdpuyhy@163.com; qingsongchen@aliyun.com

NF-κB can lead to chronic inflammation, carcinogenesis, and autoimmune diseases[24], and is a transcription factor required for inflammatory responses[25]. RelA (p65) is one of five members of the NF-κB family[26]. Chen et al. discovered upregulation of expression of the NF-κB pathway in human tendon adhesion, and that knockdown of p65 expression may be a promising approach to prevent tendon adhesions[27]. Cellular senescence induced by the proto-oncogene ras is accompanied by accumulation of p53 and p16[28]. In irregular blood flow, Piezo1 protein is activated. It mediates integrin activation *via* the $G_{q/11}$ subunit which, in turn, leads to a vascular inflammatory response mediated by NF-κB/p65 activation[29]. However, the molecular regulatory mechanisms of Piezo1 and the NF-κB/p65 pathway in HAVS are poorly understood.

Here, we aimed to address this critical knowledge gap by investigating whether the Piezo1 and NF-κB/p65 signaling pathways significantly influence vibration-induced cellular damage in vascular smooth muscle. We also aimed to determine whether angiogenic chemokines, regulated by the NF-κB/p65 signaling pathway, are associated with VWF, using both rat and cellular models and human serum samples obtained from occupational populations exposed to vibration.

Results

Vibration-induced vascular injury and increased expression of Piezo1

To investigate the effects of vibration on vascular, we exposed rat tails to vibration at 125 Hz with an acceleration of 49 m/s², with a daily vibration exposure duration of 4 h. Cluster of differentiation (CD)31 plays a protective role in maintaining vascular integrity under conditions of immune stress[30,31]. Downregulation of endomucin (EMCN) expression promotes neutrophil migration, thereby exacerbating injury[32]. We found that expression of EMCN and CD31 in the ventral tail artery of rats decreased in a time-dependent manner after vibration exposure (Fig. 1a). Under a transmission electron microscope (TEM), observations of smooth muscle cells from the ventral tail artery revealed structural and functional damage after exposure to vibration, which was correlated with the duration of exposure (Supplementary Fig. 1). In vitro experiments, we exposed human umbilical artery smooth muscle cells (HUASMCs) to vibration at 125 Hz with an acceleration of 5.9 m/s², with vibration durations of 1 h, 2 h, 3 h, and 4 h, respectively. This vibration caused the apoptosis of HUASMCs (Fig. 1d). Then, we examined the effects of vibration on Piezo1 expression. Vibration upregulated Piezo1 expression in arterial vascular smooth muscle cells in tails compared with tails not exposed to vibration (Fig. 1e, f). Piezo1 expression in HUASMCs increased after vibration (Fig. 1g). These results suggested that vibration leads to vascular injury and apoptosis of vascular smooth muscle cells in rat tails, and that exposure increases the expression of Piezo1.

Vibration stimulates Piezo1 overexpression and Piezo1-dependent Ca^{2+} influx in HUASMCs

We investigated whether vibration affects the upregulation of Piezo1 expression. First, we measured the protein expression of Piezo1 in HUASMCs exposed to different durations of contact vibrations. We discovered that vibration upregulated Piezo1 expression (Supplementary Fig. 2a). Piezo1 is a transmembrane ion channel. Hence, we used a Ca^{2+}-sensitive fluorescent dye (Fluo-4) to investigate whether different durations of vibration affected Ca^{2+} influx in HUASMCs. Vibration promoted an increase in the intracellular Ca^{2+} concentration (Fig. 2a, b). Next, we used the Piezo1 antagonist GsMTx4 to investigate if Ca^{2+} influx in HUASMCs was associated with Piezo1. GsMTx4 treatment inhibited vibration-induced accumulation of intracellular Ca^{2+}, suggesting Piezo1-mediated Ca^{2+} in HUASMCs exposed to vibration (Fig. 2c, d). We also undertook western blotting to explore if Piezo1 is associated with vibration. Expression of Piezo1, p53, and p65 was upregulated after vibration. Unsurprisingly, GsMTx4 treatment inhibited attenuated (or even reversed) the phenomena stated above (Fig. 2e, f). These results suggested that vibration could promote Piezo1 expression and Piezo1-mediated Ca^{2+} influx in HUASMCs, and that cellular dysfunction induced by vibration could be alleviated using GsMTx4.

Knockdown of Piezo1 expression inhibits vibration-induced dysfunction in HUASMCs

Next, we specifically knocked down Piezo1 expression in HUASMC using siRNA technology to explore the association of Piezo1 with vibration (Fig. 3a, b). Ca^{2+} influx after vibration was observed in HUASMCs, but the increase in intracellular Ca^{2+} concentration was reduced after specific knockdown of Piezo1 expression (Fig. 3c, d) Western blotting showed that the changes in the knockdown of the Piezo1 group were opposite to those in the NC group (Fig. 3e, f). Also, vibration-induced increased expression of p65, and the extent of this increase was reduced slightly after knockdown of Piezo1 expression.

Upregulation of Piezo1 expression by vibration induced may be synchronized with the NF-κB/p65 signaling pathway

We wished to ascertain the essential role of Piezo1 in the progression and development of HAVS. PROMO-ALGGEN v8.3 (https://alggen.lsi.upc.es/cgi-bin/promo_v3/promo/promo.cgi?calledBy=alggen&dirDB=TF_8.3/) and the Cistrome DB Toolkit (http://cistrome.org/db/) were used to locate the putative transcription start site (TSS) in the Piezo1 promoter sequence. By cross-analyzing the transcription factors screened by two methods, we found a high potential for the involvement of RelA/p65 and NF-κB in regulation through screening (Fig. 4a–c). To ascertain if RelA/p65 is associated with vibration-induced vascular injury, we measured p65 expression in rat and cell models. p65 expression was increased significantly in vibration-induced rat caudal vessels (Fig. 4d, e). mRNA expression of p65 in HUAMCs was increased in the vibration group compared with that in the control group (Fig. 4f). The results stated above were consistent with the data of virtual screening of the database. Hence, during vibration, Piezo1 may cause vascular injury through p65 possibly through the NF-κB/p65 signaling pathway.

Increased levels of NF-κB/p65-related chemokines in the plasma of patients exposed to vibration and in a rat model of vibration exposure

We collected blood samples from occupational groups in a factory in Zhongshan City. We categorized them into three groups according to whether they were exposed to HTV or not, and whether VWF occurred or not, respectively: control, non-VWF, and VWF. Piezo1 could not be detected in blood samples, so we searched for assays related to the NF-κB/p65 signaling pathway by TRRUST v2. NF-κB can target inflammation directly by increasing the production of chemokines[33]. Based on TRRUST v2, we found expression of CCL2, CCL5, CXCL1, CXCL2, and CXCL10 to be regulated by NF-κB/p65 (Fig. 5a). Using ELISAs to detect the chemokines, we found that expression of CCL2, CCL5, CXCL1, CXCL2, and CXCL10 ($P < 0.001$ for all factors) was higher in the non-VWF group relative to the control group. Blood samples contained higher expression of chemokines in the VWF group compared with that in the non-VWF group (Fig. 5b). Analysis of receiver operating characteristic (ROC) curves was done to assess the sensitivity of vascular chemokines to recognize VWF (Fig. 5c). Of the five modulators tested, CCL2 had the highest area under the ROC curve (AUC) of 0.964 (95% CI, 0.929–0.999; $P < 0.001$), with a Youden Index of 0.900 and critical value of 268.279 pg/mL. AUC > 0.90 was documented for CCL5, CXCL1, CXCL2, and CXCL10 ($P < 0.001$) (Supplementary Table 1). Expression of these chemokines increased in a time-dependent manner in a vibration model in rats (Fig. 5d). These results suggested that chemokine expression in plasma was increased significantly in patients with VWF and in rats exposed to vibration.

NF-κB/p65-related angiogenic chemokine expression associated with vibration exposure

Vibration could upregulate the expression of chemokines in HUASMCs (Fig. 6a, b). Next, we specifically knocked down p65 expression in HUASMC using siRNA technology to explore the association of p65

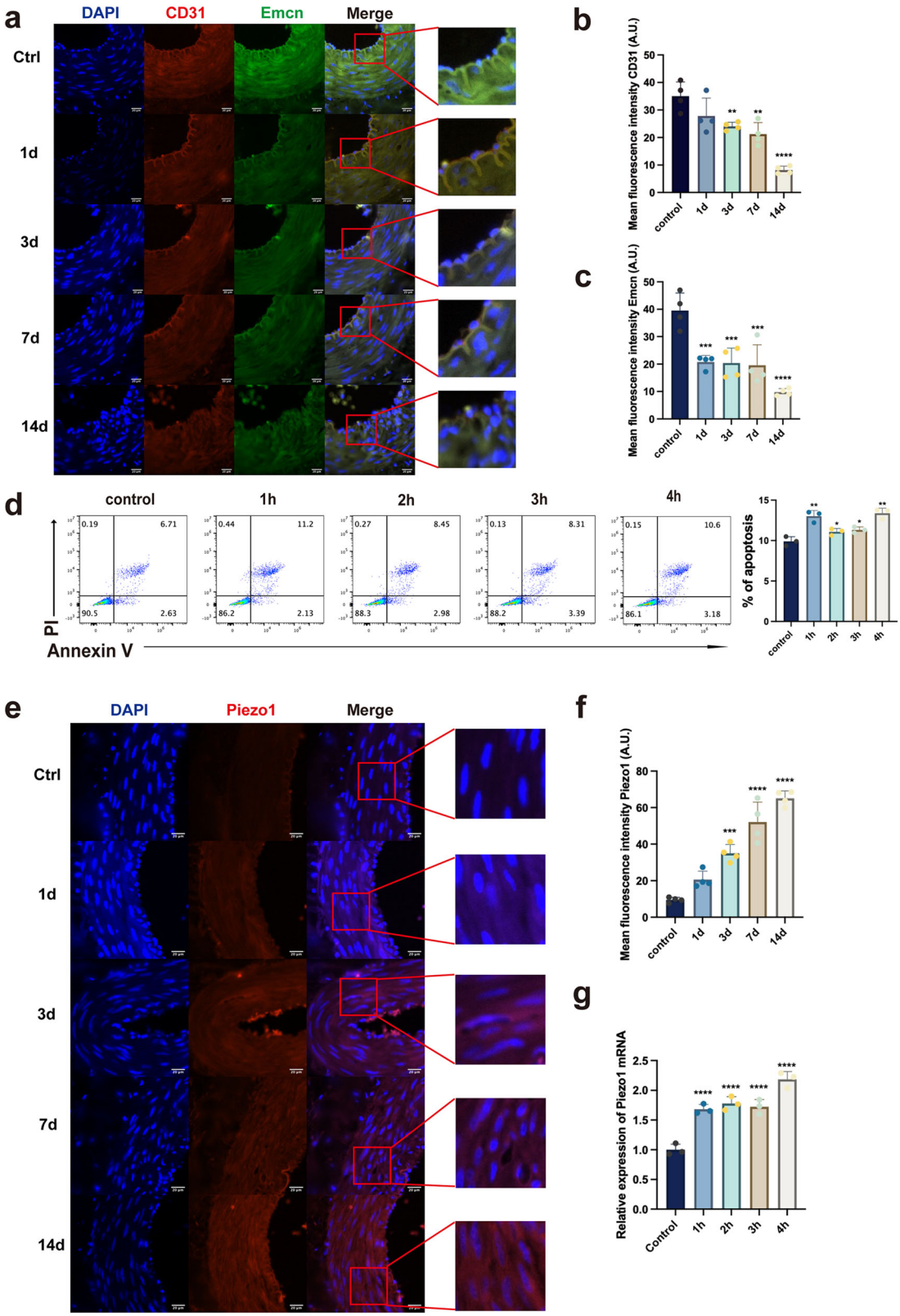

Fig. 1 | Piezo1 is upregulated in vibration-induced arterial vascular smooth muscle cells of rat tails and HUASMCs. a Representative image of CD31 and EMCN immunofluorescence (IF) staining in the ventral tail artery of rats exposed to Ctrl (0 d), 1 d, 3 d, 7 d, or 14 d vibration. The ventral tail artery are stained with DAPI (blue), CD31 (red), and Emcn (green). Scale bar: 20 μm. **b** The graph shows the mean fluorescence intensity of CD31 ($n = 4$). **c** The graph shows the mean fluorescence intensity of Emcn ($n = 4$). **d** HUASMCs were collected after control (0 h), 1 h, 2 h, 3 h, or 4 h vibration exposed, stained with Annexin V/PI, and then used for flow cytometry analysis. The graph shows the percentage of apoptosis cells in control (0 h), 1 h, 2 h, 3 h, and 4 h vibration group. The results are expressed as the means with SD ($n = 3$). **e** Representative images of Piezo1 IF staining in the ventral tail artery of rats exposed to Ctrl (0 d), 1 d, 3 d, 7 d, or 14 d vibration. The ventral tail artery are stained with DAPI (blue) and Piezo1 (Red). Scale bar: 20 μm. **f** The graph shows the mean fluorescence intensity of Piezo1 ($n = 4$). **g** qRT-PCR analysis of Piezo1 expression in HUASMCs with 0 h, 1 h, 2 h, 3 h or 4 h vibration. The experiment was repeated thrice, $^{*}P < 0.05$, $^{**}P < 0.01$, $^{***}P < 0.001$, $^{****}P < 0.0001$. One-way ANOVA is used for analysis.

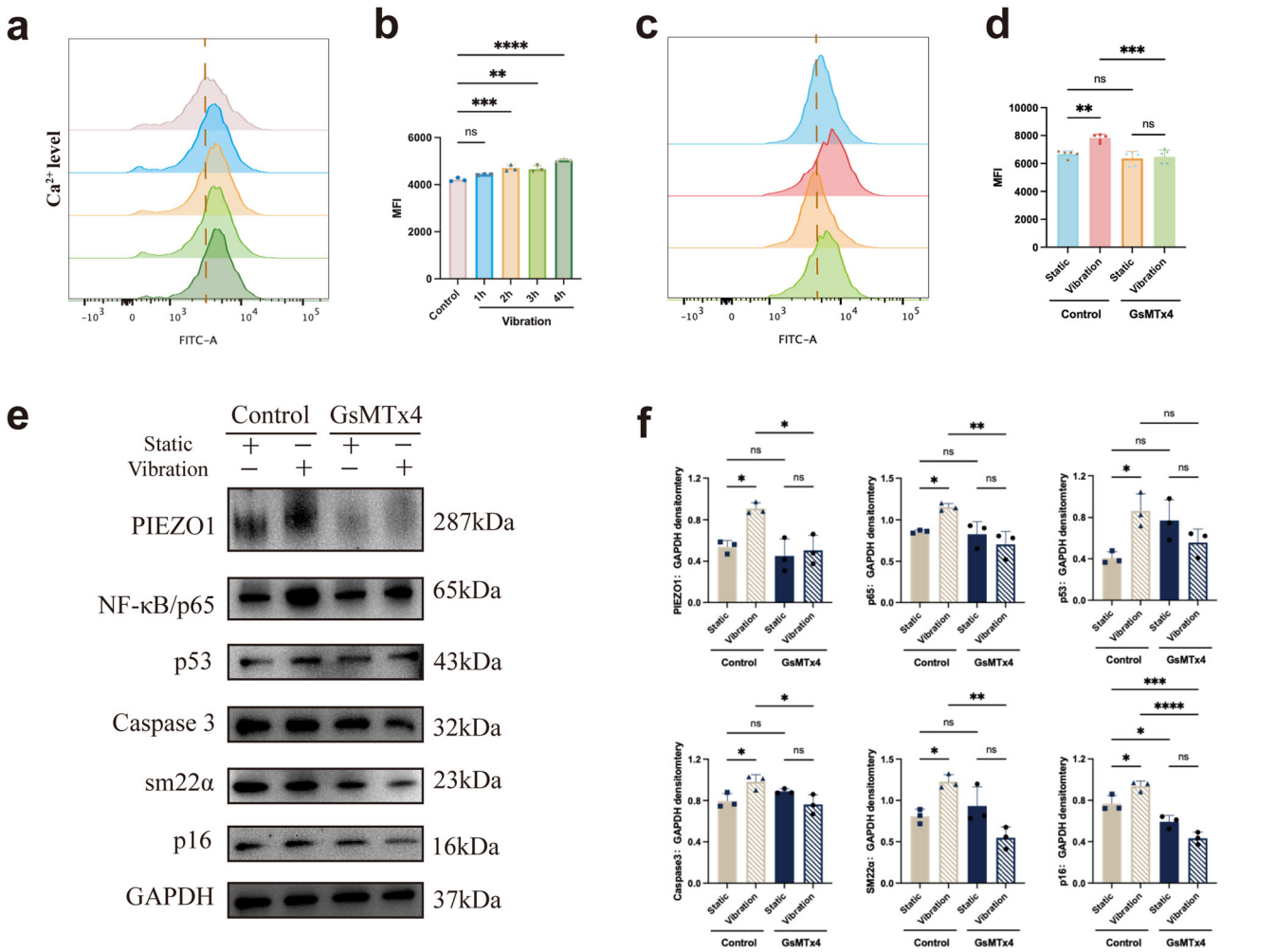

Fig. 2 | Piezo1 expression and Piezo1-dependent calcium influx in HUASMCs subjected to vibration. **a** Ca^{2+} levels in HUASMC exposed to 0 h, 1 h, 2 h, 3 h, or 4 h vibration were detected by flow cytometry. **b** Ca^{2+} levels are indicated by the mean fluorescence intensity ($n = 3$). **c** Ca^{2+} levels in HUASMC measured by flow cytometry of the Control-Static group, Control-Vibration group, GsMTx4-Static group, and GsMTx4-Vibration group. **d** Ca^{2+} levels are indicated by the mean fluorescence intensity ($n = 3$). **e** Representative images of western blot of Piezo1, NF-κB/p65, p53, Caspase 3, sm22α, p16 and GAPDH in the Control-Static group, Control-Vibration group, GsMTx4-Static group, and GsMTx4-Vibration group. **f** Statistical analysis with results normalized using corresponding internal reference proteins. The experiment was repeated thrice, $^{*}P < 0.05$, $^{**}P < 0.01$, $^{***}P < 0.001$, $^{****}P < 0.0001$. One-way ANOVA is used for analysis.

with vibration (Fig. 6c). The increase in intracellular Ca^{2+} concentration after re-exposure to vibration after specific knockdown of p65 expression in HUASMCs was reduced compared with that in the untreated group (Fig. 6d). Western blotting showed that vibration-induced changes could be alleviated or reversed after knockdown of p65 expression (Fig. 6e, f). Vibration could lead to dysfunction of HUASMCs through the NF-κB/p65 signaling pathway, which is closely related to Piezo1 activation.

Discussion

Taken together, our results highlight that vibration-induced vascular injury may be mediated by Piezo1 and is associated with the expression of angiogenic chemokines. Piezo1 is a mechanosensitive channel that converts applied forces into electrical signals[34]. Recent evidence suggests that Piezo1 channels act as receptors for shear and tensile stresses, and mediate various mechanotransduction pathways necessary for regulating cardiovascular physiology[35,36]. Our study demonstrates that vibration is likely translated into biological signaling via Piezo1, leading to vascular dysfunction-associated phenotypes and downstream high expression of chemokines. Importantly, we also found that Piezo1-associated angiogenic chemokine expression in blood samples from occupational populations was elevated in vibration-exposed individuals and reached even higher levels in those who developed VWF. Thus, this is the first report emphasizing the role of Piezo1 in the progression of vibration-induced vascular injury. Additionally, angiogenic chemokines downstream of Piezo1 can serve as potential biomarkers for early diagnosis of HAVS.

HTV is commonly simulated using the rat-tail model[37–39]. Under TEM, observations of smooth muscle cells in the rat tail ventral artery revealed that as vibration exposure increases, the structure and function of smooth muscle cells progressively deteriorate, causing varying degrees of damage to different organelles. The ventral artery injury in rat tails decreased expression of EMCN and CD31 and increased Piezo1 expression, with increasing duration of vibration exposure. Expression of endomucin (EMCN) and cluster of differentiation (CD)31 contributes to vascular angiogenesis, and their functional decline underlies impaired in diabetic nonhealing wounds[40,41]. Subsequently, through bioinformatics analysis, we discovered that NF-κB/p65 serves as a transcription start site (TSS) for Piezo1, and that suppressing p65 expression in HUASMCs elicited similar effects to those observed after inhibiting Piezo1 expression. NF-κB can target inflammation directly by increasing the production of chemokines[33]. Following this, we screened five angiogenic chemokines within the NF-κB/p65 signaling pathway: CCL2, CCL5, CXCL1, CXCL2, and CXCL10. Numerous studies have also indicated that five chemokines are associated with the NF-κB signaling pathway[42–46]. We found that the expression of these chemokines

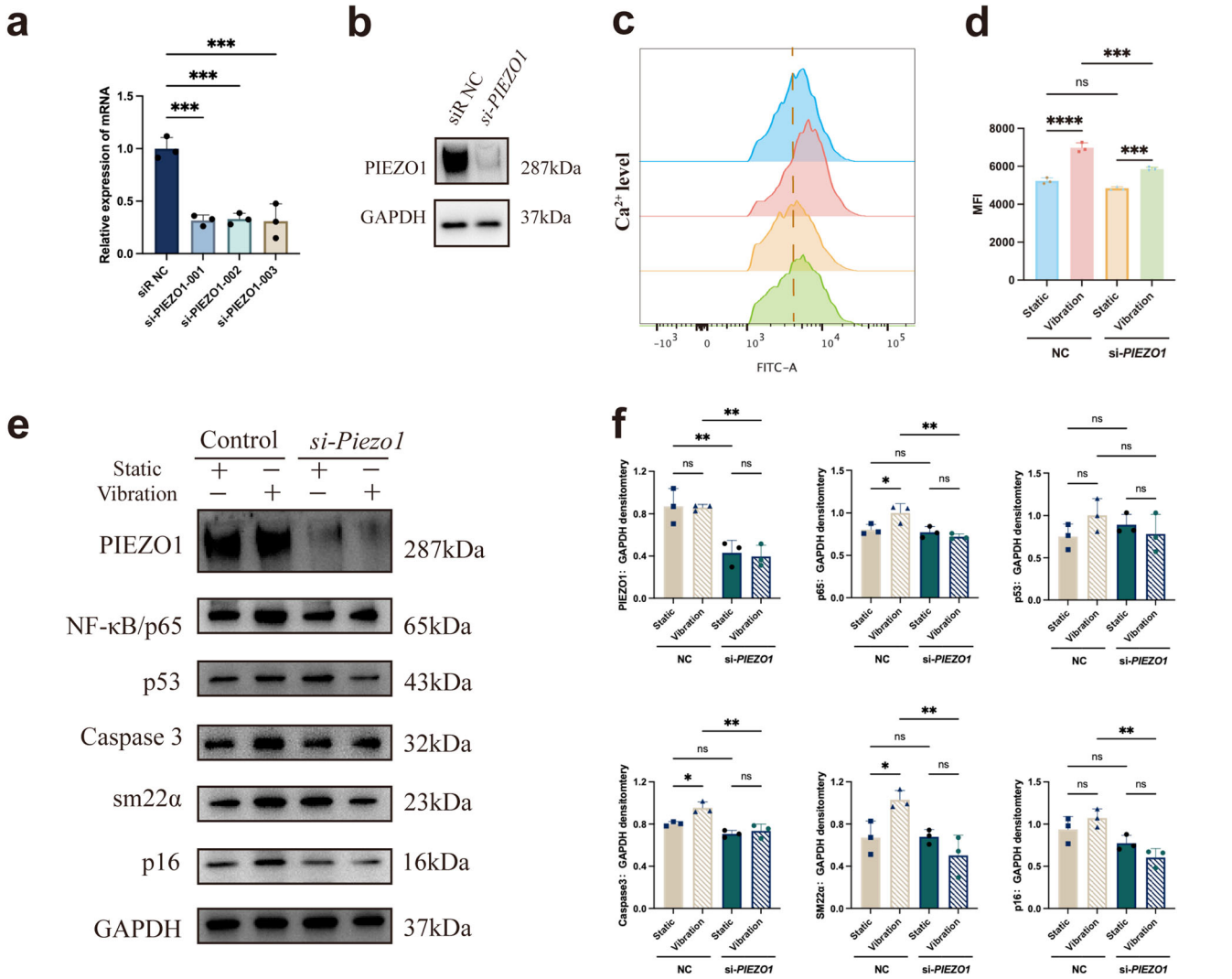

Fig. 3 | Knockdown of Piezo1 inhibits vibration-induced cellular dysfunction in HUASMCs. a HUASMCs were transfected by si-*NC*, *si-PIEZO1*-001, *si-PIEZO1*-002 and *si-PIEZO1*-003 after 48 h, Piezo1 was measured by qRT-PCR ($n = 3$). **b** Piezo1 was measured by western blotting after being transfected by *si-PIEZO1*-001. **c** Ca^{2+} levels in HUASMC measured by flow cytometry of the NC-Static group, NC-Vibration group, *si-PIEZO1*-Static group, and *si-PIEZO1*-Vibration group. **d** Ca^{2+} levels are indicated by the mean fluorescence intensity ($n = 3$). **e** Representative images of western blot of Piezo1, NF-κB/p65, p53, Caspase 3, sm22α, p16 and GAPDH in the NC-Static group, NC-Vibration group, *si-PIEZO1*-Static group, and *si-PIEZO1*-Vibration group. **f** Statistical analysis with results normalized using corresponding internal reference proteins. The experiment was repeated thrice, $^{*}P < 0.05$, $^{**}P < 0.01$, $^{***}P < 0.001$, $^{****}P < 0.0001$. One-way ANOVA is used for analysis.

was upregulated in association with vibration exposure in occupational groups, rats, and HUASMCs.

Chemokines are a superfamily of secreted proteins involved in immune regulation and inflammatory processes. Piezo1 has been shown to promote the production of chemokines such as CXCL2 and CXCL10, and chemokines can recruit neutrophils to migrate to a lesion and aggravate the inflammatory response[47]. Senescent vascular smooth muscle cells can secrete chemokines, thereby forming a pro-inflammatory microenvironment that aids local inflammation in vascular tissues[48]. Analysis of ROC curves revealed that chemokines could be used as predictors of VWF in occupational groups. The functional role of Piezo1 in mechanotransduction and various diseases makes it a potential target for therapeutic intervention[49–51]. Our study suggests that Piezo1 may be a promising modality for the treatment of HAVS, and further studies will be conducted to assess its therapeutic potential in humans. However, the success of targeting Piezo1 in therapy will depend on several factors, including the specific disease or condition being targeted, as well as the interactions of Piezo1 with other proteins and signaling pathways.

The NF-κB pathway provides many targets for the development of specific drugs for the treatment of inflammatory diseases[52]. It has been shown that NF-κB/p65 acts as a tumor suppressor and, thus, maintains cells in a senescent state, whereas loss of p53 or p16 is associated with senescence bypass[53,54]. For example, cellular senescence induced by the proto-oncogene ras is accompanied by the accumulation of p53 and p16[28]. Smooth muscle (SM)22α protein is a smooth muscle-specific marker that is found predominantly in mature smooth muscle cells, and SM22α expression is increased in senescent cells[55]. The ageing cell develops increasingly complex phenotypes that have beneficial and detrimental effects upon the health of the organism[56]. We found that vibration upregulated the expression of p53, p16, and SM22α in HUASMCs, and could be alleviated by knockdown p65 expression.

While our findings provide insights into the mechanisms of HAVS, several limitations must be acknowledged. The inability to directly detect Piezo1 in human samples necessitates the use of animal and cell models, which may not fully recapitulate the human disease. The pathology of vascular diseases involves the activation of multiple cell types, including smooth muscle cells (SMCs), immune cells (such as macrophages and T cells), and endothelial cells, among others[57].Piezo1 in endothelial and neutrophil cells has been found to act as a mechanosensor mediating shear stress-induced vascular pathological activation[58,59]. The transcriptional

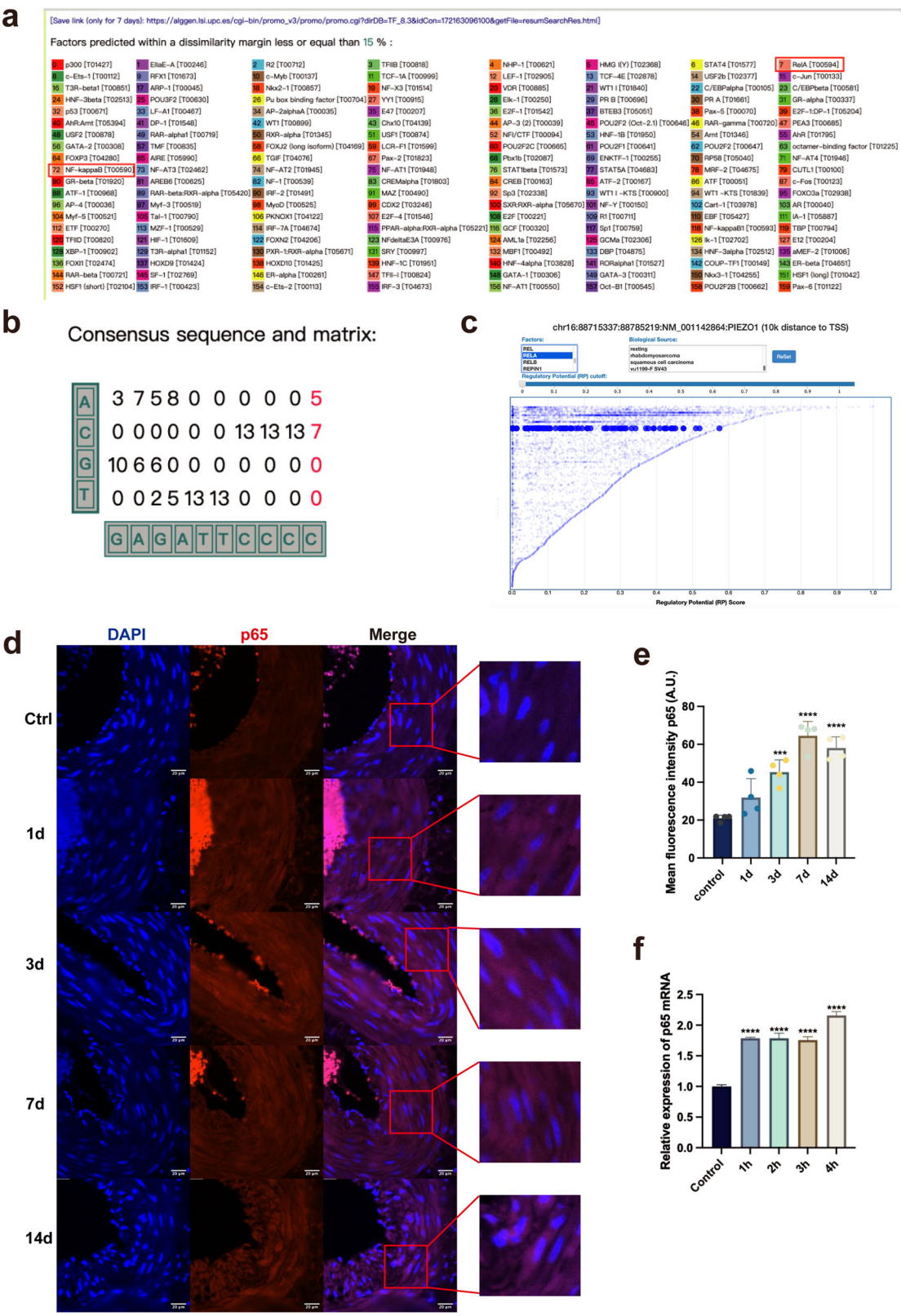

Fig. 4 | NF-κB/p65 signaling pathway is responsible for the transcription of Piezo1. a The PROMO project of ALGGEN was used to locate the identification of the putative transcription start site (TSS) in the Piezo1 promoter sequence. **b** The consensus sequence and matrix about RelA/p65 with Piezo1. **c** Cistrome DB Toolkit was used to identify the transcription factors of Piezo1. **d** Representative images of NF-κB/p65 IF staining in the ventral tail artery of rats exposed to Ctrl (0 d), 1 d, 3 d, 7 d, or 14 d vibration. The ventral tail artery are stained with DAPI (blue) and p65 (Red). Scale bar: 20 μm. **e** The graph shows the mean fluorescence intensity of p65 ($n = 4$). **f** qRT-PCR analysis of p65 expression in HUASMCs with 0 h, 1 h, 2 h, 3 h or 4 h vibration. The experiment was repeated thrice, $^{*}P < 0.05$, $^{**}P < 0.01$, $^{***}P < 0.001$, $^{****}P < 0.0001$. One-way ANOVA is used for analysis.

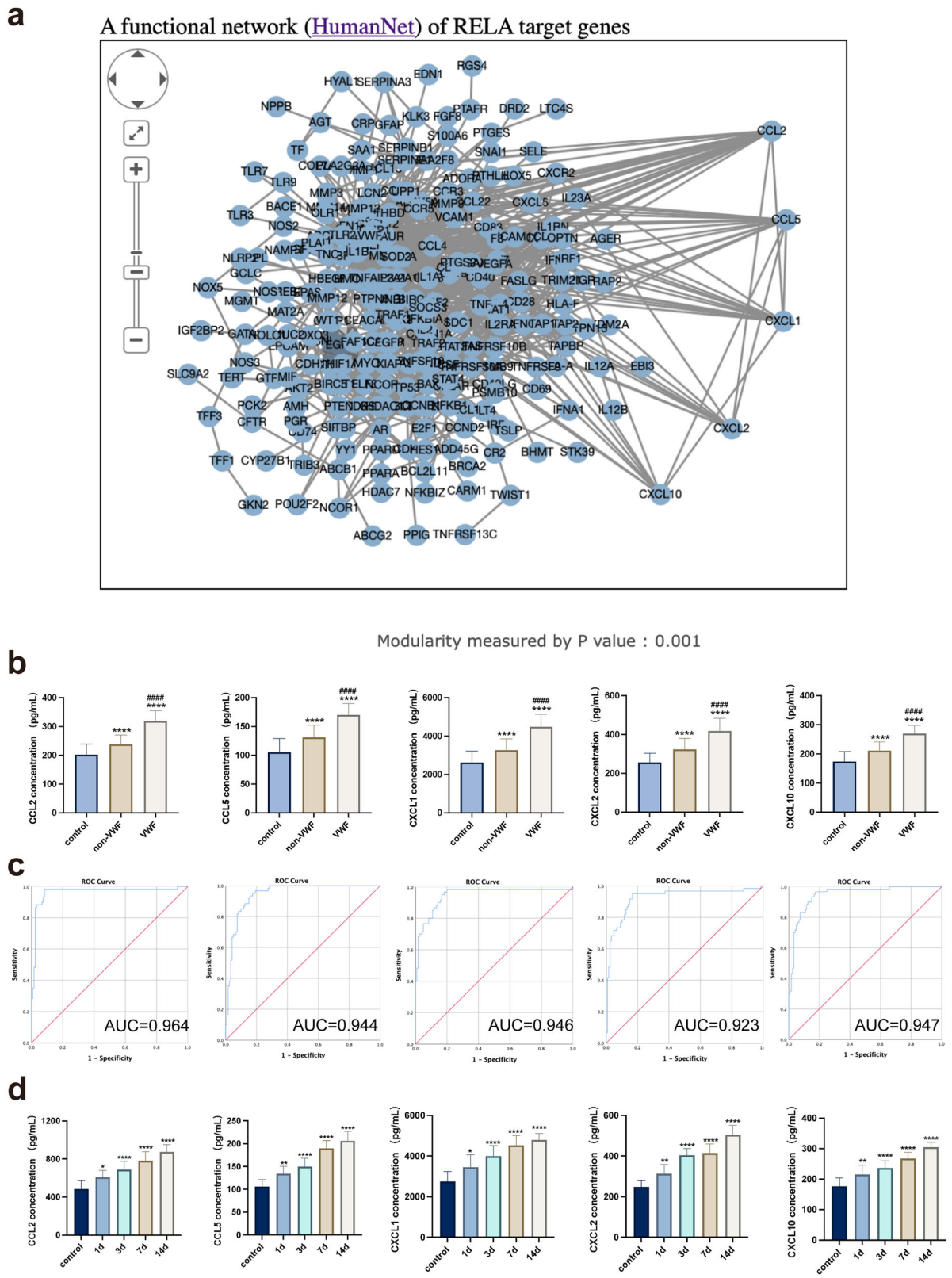

Fig. 5 | Elevated levels of NF-κB/p65-related chemokines in the blood of patients exposed to vibration and a rat model of vibration exposure. a TRRUST v2 was used to build a functional network of RelA/p65 target genes ($P < 0.001$). **b** Plasma chemokine levels were measured in three occupational groups by ELISAs ($n = 60$ per group). **c** Area under the corresponding ROC curve for chemokines predicting the occurrence of VWF in an occupational population ($n = 180$). **d** Changes in plasma chemokine levels after exposure of rat tails to 0 d, 1 d, 3 d, 7 d, or 14 d vibrations. $^{*}P < 0.05$, $^{**}P < 0.01$, $^{***}P < 0.001$, $^{****}P < 0.0001$. $^{\#\#\#\#}$, Comparison between VWF group and non-VWF group, $P < 0.0001$. One-way ANOVA is used for analysis.

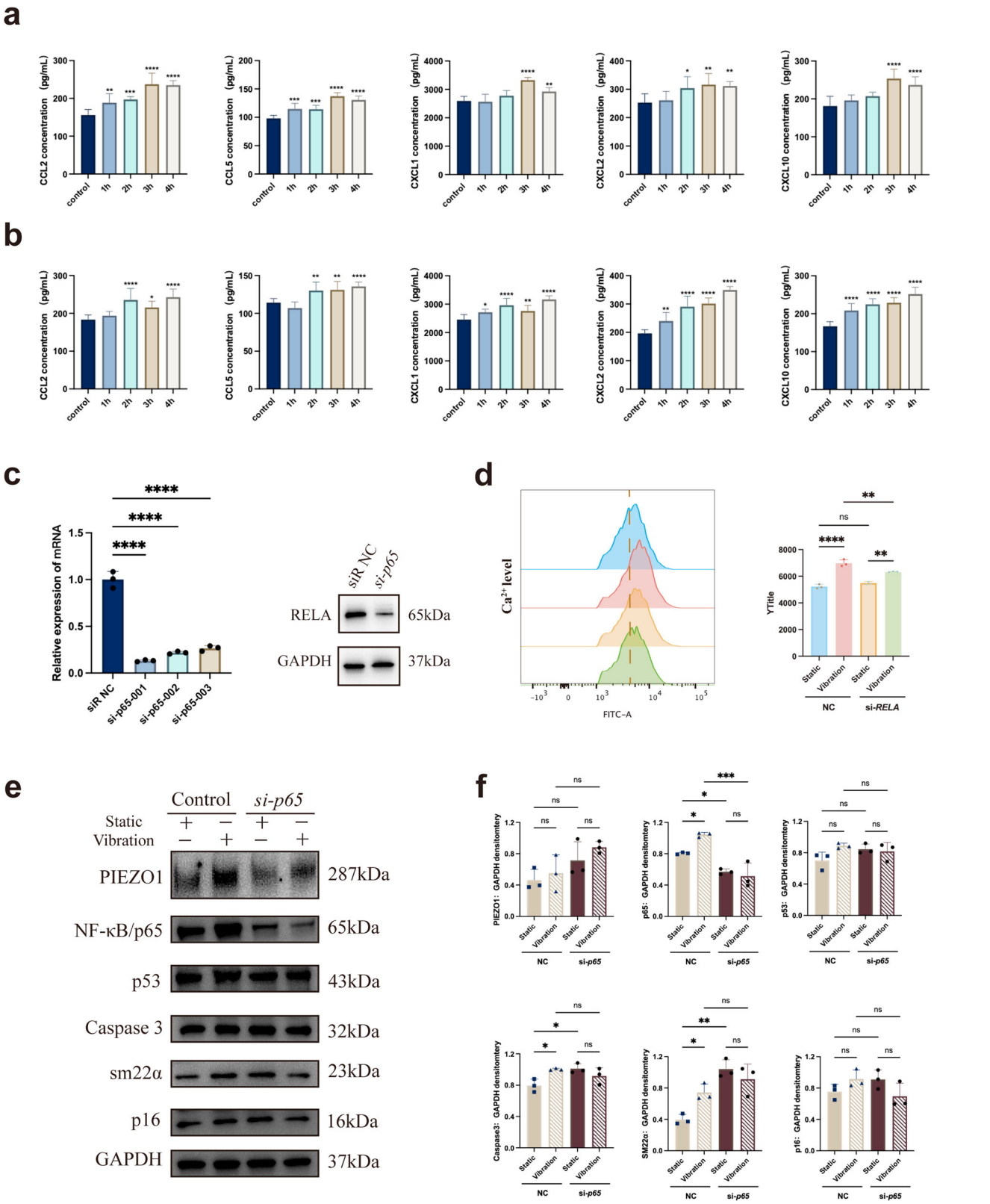

Fig. 6 | Knockdown of p65 inhibits vibration induced cellular dysfunction in HUASMCs. a Changes in chemokine levels in culture supernatants of HUASMCs after exposure to 0 h, 1 h, 2 h, 3 h, or 4 h of vibration. **b** Changes in chemokine levels in cell lysates of HUASMC after exposure to 0 h, 1 h, 2 h, 3 h, or 4 h of vibration. **c** HUASMCs were transfected by *si*-NC, *si-p65-001*, *si- p65-002* and *si- p65-003* after 48 h, p65 was measured by qRT-PCR ($n = 3$). p65 was measured by western blotting after being transfected by *si-p65-001*. **d** Ca^{2+} levels in HUASMCs were measured by flow cytometry of the NC-Static group, NC-Vibration group, *si-p65*-Static group, and *si-p65*-Vibration group. Ca^{2+} levels are indicated by the mean fluorescence intensity ($n = 3$). **e** Representative images of western blot of Piezo1, NF-κB/p65, p53, Caspase 3, sm22α, p16 and GAPDH in the NC-Static group, NC-Vibration group, si-p65-Static group, and si-p65-Vibration group. **f** Statistical analysis with results normalized using corresponding internal reference proteins. The experiment was repeated thrice, $^{*}P < 0.05$, $^{**}P < 0.01$, $^{***}P < 0.001$, $^{****}P < 0.0001$. One-way ANOVA is used for analysis.

Table 1 | Data comparison from an occupational-epidemiology questionnaire among three population groups

Group	Total (n = 180)	Control (n = 60)	exposed to HTV		F/x^2	P
			non-VWF (n = 60)	VWF (n = 60)		
Age ('x ± s)	39.85 ± 6.425	39.83 ± 6.938	39.43 ± 6.264	40.28 ± 6.123	0.261	0.771
BMI ('x ± s)	24.03 ± 4.321	23.66 ± 4.223	23.88 ± 3.029	24.54 ± 5.404	0.678	0.509
Length of service ('x ± s)	10.09 ± 6.404	9.11 ± 6.362	9.78 ± 6.464	11.37 ± 6.279	1.990	0.140
Tobacco smoking, no. (%)	–	–	–	–	1.770	0.173
Non	88 (48.9)	36 (60)	24 (40.0)	28 (46.7)		
Current	82 (45.6)	22 (36.7)	32 (53.3)	28 (46.7)		
Former	10 (5.5)	2 (3.3)	4 (6.7)	4 (6.7)		
Alcohol consumption, no. (%)	–	–	–	–	0.362	0.697
Non	94 (52.2)	35 (58.3)	32 (53.3)	27 (45.0)		
Current	83 (46.1)	24 (40.0)	27 (45.0)	32 (53.3)		
Former	3 (1.7)	1 (1.7)	1 (1.7)	1 (1.7)		
Hand symptoms, no. (%)						
Numbness	77 (42.8)	0 (0.0)	21 (35.0)	56 (96.3)	135.819	<0.001
Tingling	48 (26.7)	0 (0.0)	9 (15.0)	39 (65.0)	57.754	<0.001
Feeling cold	43 (23.9)	2 (3.3)	7 (11.7)	34 (56.7)	38.257	<0.001

VWF vibration white finger.

profiling of human endothelial cells has revealed the regulation of mechanosensitive genes by PIEZO1 and inputs from pro-oxidants and inflammatory stimuli[60]. Mild and well-controlled whole-body mechanical vibration can have a positive effect on immune responses[61]. Furthermore, while our study focused on Piezo1 and the NF-κB/p65 pathway, other signaling pathways may be also involved in process. The NF-κB signaling pathway engages in direct or indirect regulatory interactions with other signaling pathways, such as PI3K/AKT, MAPK, JAK-STAT, TGF-β, Wnt, Notch, and Hedgehog[62]. Therefore, future studies should explore the potential involvement of other signal transduction mechanisms and the roles of endothelial and immune cells in these processes.

Overall, our study highlights the crucial roles of Piezo1 and the NF-κB/p65 signaling pathway in the development of HAVS. Piezo1 may be associated with the NF-κB/p65 pathway to promote vascular chemokine release and cellular dysfunction. Increased levels of vascular chemokines may be a promising approach in the early diagnosis of HAVS, and Piezo1 may be a therapeutic target.

Methods

Ethical approval of the study protocol for human experiments

This study protocol was approved (116) by the Ethics Committee of Guangdong Pharmaceutical University (Guangdong, China) in 2021. Each person provided written informed consent to participate in this study. All ethical regulations relevant to human research participants were followed.

Grouping

One-hundred and eighty men were selected using judgment sampling from employees of the same factory in Zhongshan City (Guangdong Province, China). These participants were divided into three groups at a 1:1:1 ratio: control; vibration white finger (VWF); non-VWF (exposed to hand-transmitted vibration but without developing VWF). Specimens were excluded for any of the following reasons: cardiovascular disease, liver disease, kidney disease, diabetes mellitus, Raynaud's disease, infectious diseases, or any illness or medication taken within 2 weeks before study entry.

The demographic and clinical characteristics of the three occupational groups are presented in Table 1. Participants in the control group were workers engaged in product packaging at the same factory who were not exposed to hand-transmitted vibration (HTV). Participants in the non-VWF group and VWF group were selected from grinding posts (job positions) with exposure to hand-transmitted vibration. Among them, workers who provided photographs of vibration-induced white-finger attacks were classified into the VWF group. There were no statistically significant differences in age, body mass index (BMI), or working-age levels among the three groups *($P > 0.05$)*. There was no significant difference in the prevalence of tobacco smoking or alcohol consumption among the three groups. *($P > 0.05$)* However, the prevalence of hand numbness, finger pain, and feeling cold hands was significantly higher in the VWF group compared with those in the other two groups *($P < 0.001$)*.

Collection and processing of blood samples

Each participant underwent an overnight fast. Using a potassium heparin anticoagulation negative-pressure tube, a nurse collected 4 mL of blood from an elbow vein. Immediately after collection, each sample was mixed gently for 30 s and stored in a 4 °C incubator. Samples were sent to a laboratory and centrifuged (3000 × g, 10 min, 4 °C). Plasma was separated and dispensed into a 500-μL centrifuge tube and stored at −80 °C. For subsequent experiments, samples were allowed to thaw at room temperature.

Ethical approval of the study protocol for animal experiments

The handling of, and experimental procedures upon, animals were conducted with the approval (GDPULAC2024141) of the Laboratory Animal Ethics Committee of Guangdong Pharmaceutical University. We have complied with all relevant ethical regulations for animal use.

Animal experiments

Fifty male Sprague–Dawley rats (7–8 weeks; 216.98 ± 8.69 g) were purchased from Guangdong Medical Laboratory Animal Center (Guangdong, China). Rats were divided randomly into five groups of 10 based on body weight: control (0 d); 1 d; 3 d; 7 d; 14 d. (Supplementary Table 2) A 3% to 5% picric acid solution was used as the marking solution and applied to different body parts of the rats for marking.

The vibration system was a special instrument from CNMF Experimental Vibration Apparatus (Guangzhou, China). To ensure the stability and consistency of values for vibration exposure, rats were placed on a separate retainer (Yuzhong Xiongyan, Chongqing, China). The tail was fixed on a vibrating table with breathable adhesive tape (3 M; Saint Paul, MN, USA) to ensure contact with the vibration source. The tails of rats were

vibrated at 125 Hz with an acceleration of 49 m/s^2. Each experimental session was conducted daily between 5 pm and 9 pm. Rats in the control group were positioned on the vibration table, but not exposed to vibration.

Rats were injected intraperitoneally with 3% pentobarbital sodium after vibration. After killing, rats were dissected together, and blood was collected after incising the abdominal cavity to access the aorta. Blood samples were collected in EDTA anticoagulant tubes and centrifuged (1000 × *g*, 15 min, 4 °C) Subsequently, the tubes were placed in a − 80 °C cryogenic refrigerator so that the plasma samples could be conserved to undertake enzyme-linked immunosorbent assays (ELISAs). The tail skin was cut by ~5 mm. The ventral tail artery could be identified in the ventral center by removing the surrounding excess skin tissue. A segment of ~1 mm^3 of the ventral tail artery was surgically removed and subjected to pre-fixation processing for subsequent experiments.

Cell culture

Human umbilical artery smooth muscle cells (HUASMCs) were purchased from (Cellverse, Shanghai, China). Cells were cultured in the iCell™ primary smooth muscle cell culture system (Cellverse, Shanghai, China) containing 10% fetal bovine serum (FBS) and 1% penicillin/streptomycin. Then, they were cultured in 25-cm^2 culture flasks in a humidified atmosphere at 37 °C in an atmosphere of 5% CO_2.

RNA extraction and real-time reverse transcription-quantitative polymerase chain reaction (RT-qPCR)

Total RNA was isolated from cells using TRIzol® Reagent (TaKaRa Biotechnology, Shiga, Japan) according to manufacturer instructions. Reverse transcription was undertaken using total RNA (1000 ng) and the PrimeScript™ RT Reagent Kit (TaKaRa Biotechnology). RT-qPCR amplification was assessed in the StepOnePlus™ Real-Time PCR System (Thermo Fisher Scientific, Waltham, MA, USA) using the SYBR™ Premix Ex Taq II kit (TaKaRa Biotechnology). The cycling conditions were: 95 °C for 30 s, followed by 40 cycles of 95 °C for 5 s, and 60 °C for 30 s. All PCRs were carried out in duplicate and normalized to the internal reference (glyceraldehyde 3-phosphate dehydrogenase (GAPDH) for mRNAs. The $2^{-\triangle\triangle Ct}$ method was used to evaluate relative mRNA expression. The primers we employed are listed in Supplementary Table 3.

Immunofluorescence staining

Tail tissues were fixed in 4% paraformaldehyde fixative solution at 4 °C for 24 h, and then dehydrated in a 30% sucrose solution for 3 days. Coronal sections of thickness 20 μm were obtained using a cryostat. Tissue sections were incubated in a solution containing phosphate-buffered saline (PBS; 0.01 M), 0.3% Triton X-100, and 3% goat serum on a shaker at room temperature for 1 h. Sections were incubated overnight at 4 °C with primary antibodies (obtained from Proteintech, Wuhan, China) diluted in goat serum. The primary antibodies used were: PIEZO1 (1:200 dilution; catalog number: 15939-1-AP), nuclear factor-kappa B (NF-κB) p65 (1:200; 10745-1-AP), endomucin (1:200; 67854-1-Ig), and cluster of differentiation (CD)31 (1:3000 28083-1-AP). The next day, sections were washed four times (10-min each time) on a shaker with Tris-buffered saline-Triton X (TBST) to remove nonspecifically bound antibodies. Fluorescent secondary antibodies were added, and sections were incubated on a shaker in the dark for 2 h at room temperature. Finally, the sections were mounted with an anti-fading mounting medium, dried in the dark, and photographed under a fluorescence microscope (Olympus, Tokyo, Japan) to measure the fluorescence intensity of the ventral tail artery. Each section was photographed and counted (×200 magnification) selecting the field of view of the ventral tail artery.

Small interfering (si)RNA transfection and cell treatments

HUASMCs were seeded in six-well plates. The confluence of HUASMCs reached ~70% after 12 h. Then, HUASMCs were transfected with a PIEZO1 mimic and negative control (Ribobio, Guangzhou, China) at a concentration of 30 nM using Lipofectamine™ 3000 reagents (Invitrogen, Carlsbad, CA, USA) according to manufacturer instructions. The Piezo1 inhibitor GsMTx4 (5 μM; ab141871; Abcam, Cambridge, UK) was added to the culture medium for cultivation for 24 h before being harvested. After 48 h of transfection, cells were collected and were used for experiments. All siRNA sequences were listed in Supplementary Table 4.

Western blotting

Proteins were extracted from HUASMCs by RIPA buffer (Beyotime Institute of Biotechnology, Shanghai, China). Protein concentrations were quantified by a bicinchoninic acid (BCA) protein assay kit (Thermo Fisher Scientific). Protein components were separated by sodium dodecyl sulfate-polyacrylamide electrophoresis using polyacrylamide gels (4–12%) and transferred onto polyvinylidene fluoride (PVDF) membranes (Immobilon P; Millipore, Burlington, MA, USA). PVDF membranes were blocked in TBST containing 5% nonfat skimmed milk and probed for 2 h. Then, PVDF membranes were incubated with primary antibodies against anti-FAM38A/PIEZO1 antibody (rabbit; 1:1000; ab 259949; Abcam), anti-NF-κB p65 antibody (rabbit; 1:1000, ab32536; Abcam), anti-p53 antibody (rabbit 1:1000, ab32049; Abcam), anti-caspase-3 antibody (rabbit; 1:5000; ab32351; Abcam), anti- smooth muscle 22 alpha (SM22)-alpha antibody (rabbit; 1:1000; 10493-1-AP; Proteintech), anti-ARPC5/p16 antibody (rabbit; 1:5000; ab51243; Abcam), or anti-GAPDH antibody (rabbit; 1:10000, 10494-1-AP; Proteintech) overnight at 4 °C. Next, PVDF membranes were incubated with secondary antibody (sheep anti-rabbit; 1:20000; ab6721; Abcam) for 1 h at room temperature. Blots were washed with TBST and underwent enhanced chemiluminescence (ECL) imaging using an ECL system (Merck Millipore, Waltham, MA, USA) and chemiluminescence system (Tanon, Shanghai, China). Blots were processed using Image Lab (Bio-Rad Laboratories, Hercules, CA, USA).

Apoptosis detection

Apoptosis was detected using an Annexin V-FITC apoptosis detection kit (Beyotime Institute of Biotechnology) according to manufacturer instructions. Briefly, we collected cells at the end of the vibration and reliquefied them in 195 μL of binding buffer. Next, 5 μL of membrane-associated protein Annexin V- fluorescein isothiocyanate (FITC) and 10 μL of PI were ligated and then incubated in the dark for 15 min. Finally, 400 μL of binding buffer was mixed and blended, and apoptosis was assessed by flow cytometry using FACSAria III, Becton Dickinson, Franklin Lakes, NJ, USA). Measurements of apoptosis intensity were analyzed using FlowJo 10.8.1 (www.flowjo.com).

Measurement of intracellular Ca^{2+} concentration

The intracellular Ca^{2+} concentration was measured by flow cytometry utilizing Fluo-4 AM (Beyotime Institute of Biotechnology). Cells were collected and washed with PBS before being stained with Fluo-4 AM (500 μL; excitation = 490 nm; emission = 525 nm) for 30 min at 37 °C. Then, cells were washed with PBS, resuspended by adding assay buffer, and analyzed by flow cytometry using FACSAria III. Measurements of mean fluorescent intensity were made using FlowJo10.8.1.

Bioinformatics analysis

The transcription factor binding sites (TFBSs) in the Piezo1 promoter (−1000 to +100 relative to TSS) were identified using ALGGEN-PROMO (https://alggen.lsi.upc.es/cgi-bin/promo_v3/promo/promo.cgi?calledBy=alggen&dirDB=TF_8.3/) and Cistrome Data Browser (http://cistrome.org/db/). To identify substantial changes at the transcriptional level and to gain in-depth understanding of the regulatory role of RelA/p65, we used the hub gene to introduce TRRUST v2. (www.grnpedia.org/trrust/).

ELISA

Expression of monocyte chemoattractant protein-1/C-C motif ligand 2 (MCP-1/CCL2)(MM-1552H1), macrophage inflammatory protein-2/C-X-C motif chemokine ligand 2 (MIP-2/CXCL2)(MM-0140H1), CXCL1(MM-1850H1), CXCL10(MM-2166H1), and CCL5/regulated upon activation, normal t-cell expressed, and secreted (RANTES)

(MM-0097H1) in the plasma of the three occupational groups were measured using ELISA kits (Meimian, Jiangsu, China). The concentration of MCP-1/CCL2 (MM-0099R2), MIP-2/CXCL2 (MM-0106R2), CXCL1(MM-70081R2), CXCL10(MM-72068R2), and CCL5(MM-0120R1) in the plasma of rats was detected according to manufacturer instructions. The lysates and supernatants of HUASMCs were collected and assayed using the same kits.

Statistics and reproducibility

Data from at least three independent biological replicates were reported as the mean ± SD. Statistical analyses were completed with Prism 9.5.1 (GraphPad, San Diego, CA, USA) and SPSS 26.0 (IBM, Armonk, NY, USA). The unpaired Student's *t*-test (for two groups), and one-way or two-way ANOVA (for multiple groups) were used, followed by Tukey's test. $P < 0.05$ was considered significant.

Reporting summary

Further information on research design is available in the Nature Portfolio Reporting Summary linked to this article.

Data availability

The authors declare that the data supporting the findings of this study are available within the paper and its Supplementary Information files. The numerical source data can be found in Supplementary Data. All relevant data are available from the authors upon request.

Received: 29 August 2024; Accepted: 13 January 2025;
Published online: 21 January 2025

References

1. Heaver, C. et al. Hand-arm vibration syndrome: a common occupational hazard in industrialized countries. *J. Hand Surg. Eur.* **36**, 354–363 (2011).
2. Taylor, W. The hand-arm vibration syndrome—diagnosis, assessment and objective tests: a review. *J. R. Soc. Med.* **86**, 101–103 (1993).
3. Burström, L. et al. White fingers, cold environment, and vibration–exposure among Swedish construction workers. *Scand. J. Work Environ. Health* **36**, 509–513 (2010).
4. Yu, Z. S. et al. Epidemiologic survey of vibration syndrome among riveters, chippers and grinders in the railroad system of the People's Republic of China. *Scand. J. Work. Environ. Health.* **12**, 289–292 (1986).
5. Forsakring, A. *Vibrationsskador - En skakig historian* (AFA Forsakring, Sweden, 2018).
6. International Organization for Standardization. *Mechanical Vibration And Shock—cold Provocation Tests for the Assessment of Peripheral Vascular Function—Part 1: Measurement and Evaluation of Finger Skin Temperature*. International Standard, ISO 14835-1 (ISO, Geneva, 2005).
7. Krajnak, K. et al. Recovery of vascular function after exposure to a single bout of segmental vibration. *J. Toxicol. Environ. Health A.* **77**, 1061–1069 (2014).
8. Tekavec, E. et al. Serum levels of biomarkers related to severity staging of Raynaud's phenomenon, neurosensory manifestations, and vibration exposure in patients with hand-arm vibration injury. *Sci. Rep.* **14**, 18128 (2024).
9. Tekavec, E. et al. Serum biomarkers in patients with hand-arm vibration injury and in controls. *Sci. Rep.* **14**, 2719 (2024).
10. Eriksson, K., Burström, L. & Nilsson, T. Blood biomarkers for vibration-induced white fingers. A case-comparison study. *Am. J. Ind. Med.* **63**, 779–786 (2020).
11. Krajnak, K. Frequency-dependent changes in mitochondrial number and generation of reactive oxygen species in a rat model of vibration-induced injury. *J. Toxicol. Environ. Health A* **83**, 20–35 (2020).
12. Curry, B. D. et al. Nifedipine pretreatment reduces vibration-induced vascular damage. *Muscle Nerve.* **32**, 639–646 (2005).
13. Wei, N. et al. Local vibration induced vascular pathological structural changes and abnormal levels of vascular damage indicators. *Microvasc. Res.* **136**, 104163 (2021).
14. Sorokin, V. et al. Role of vascular smooth muscle cell plasticity and interactions in vessel wall inflammation. *Front. Immunol.* **11**, 599415 (2020).
15. Coste, B. et al. Piezo1 and Piezo2 are essential components of distinct mechanically activated cation channels. *Science* **330**, 55–60 (2010).
16. Swiatlowska, P. et al. Hypertensive pressure mechanosensing alone triggers lipid droplet accumulation and transdifferentiation of vascular smooth muscle cells to foam cells. *Adv. Sci.* **11**, e2308686 (2024).
17. Su, S. A. et al. Cardiac Piezo1 exacerbates lethal ventricular arrhythmogenesis by linking mechanical stress with Ca^{2+} handling after myocardial infarction. *Research* **6**, 0165 (2023).
18. Zhu, W. et al. PIEZO1 mediates a mechanothrombotic pathway in diabetes. *Sci. Transl. Med.* **14**, eabk1707 (2022).
19. Yang, Y. et al. Piezo1 mediates endothelial atherogenic inflammatory responses via regulation of YAP/TAZ activation. *Hum. Cell* **35**, 51–62 (2022).
20. Ren, X. et al. Gsmtx4 alleviated osteoarthritis through Piezo1/Calcineurin/NFAT1 signaling axis under excessive mechanical strain. *Int. J. Mol. Sci.* **24**, 4022 (2023).
21. Xiang, Z. et al. Piezo1 channel exaggerates ferroptosis of nucleus pulposus cells by mediating mechanical stress-induced iron influx. *Bone Res.* **12**, 20 (2024).
22. Shinge, S. A. U. et al. Emerging Piezo1 signaling in inflammation and atherosclerosis; a potential therapeutic target. *Int. J. Biol. Sci.* **18**, 923–941 (2022).
23. Chen, L. F. & Greene, W. C. Shaping the nuclear action of NF-κB. *Nat. Rev. Mol. Cell Biol.* **5**, 392–401 (2004).
24. Yu, H. et al. Targeting NF-κB pathway for the therapy of diseases: mechanism and clinical study. *Signal Transduct. Target. Ther.* **5**, 209 (2020).
25. Taniguchi, K. & Karin, M. NF-κB, inflammation, immunity and cancer: coming of age. *Nat. Rev. Immunol.* **18**, 309–324 (2018).
26. Hayden, M. S. & Ghosh, S. Shared principles in NF-κB signaling. *Cell.* **132**, 344–362 (2008).
27. Chen, S. et al. RelA/p65 inhibition prevents tendon adhesion by modulating inflammation, cell proliferation, and apoptosis. *Cell Death Dis.* **8**, e2710 (2017).
28. Serrano, M. et al. Oncogenic ras provokes premature cell senescence associated with accumulation of p53 and p16INK4a. *Cell.* **88**, 593–602 (1997).
29. Albarrán-Juárez, J. et al. Piezo1 and G_q/G_{11} promote endothelial inflammation depending on flow pattern and integrin activation. *J. Exp. Med.* **215**, 2655–2672 (2018).
30. Cheung, K. et al. CD31 signals confer immune privilege to the vascular endothelium. *Proc. Natl Acad. Sci. USA* **112**, E5815–E5824 (2015).
31. Cheung, K. et al. Preservation of microvascular barrier function requires CD31 receptor-induced metabolic reprogramming. *Nat Commun.* **11**, 3595 (2020).
32. Zhang, P. et al. Endothelial Notch activation promotes neutrophil transmigration via downregulating endomucin to aggravate hepatic ischemia/reperfusion injury. *Sci China Life Sci.* **63**, 375–387 (2020).
33. Liu, T. et al. NF-κB signaling in inflammation. *Signal Transduct. Target. Ther.* **2**, 17023 (2017).
34. Lin, Y. C. et al. Force-induced conformational changes in PIEZO1. *Nature* **573**, 230–234 (2019).
35. Murthy, S. E. et al. Piezos thrive under pressure: mechanically activated ion channels in health and disease. *Nat. Rev. Mol. Cell Biol.* **18**, 771–783 (2017).
36. Harraz, O. F. et al. Piezo1 is a mechanosensor channel in central nervous system capillaries. *Circ. Res.* **130**, 1531–1546 (2022).

37. Alvarez, P., Bogen, O. & Levine, J. D. Interleukin 6 decreases nociceptor expression of the potassium channel KV1.4 in a rat model of hand-arm vibration syndrome. *Pain.* **160**, 1876–1882 (2019).
38. Alvarez, P., Bogen, O. & Levine, J. D. Nociceptor interleukin 33 receptor/ST2 signaling in vibration-induced muscle pain in the rat. *J. Pain.* **21**, 506–512 (2020).
39. Krajnak, K. et al. Applied force alters sensorineural and peripheral vascular function in a rat model of hand-arm vibration syndrome. *J. Occup. Environ. Med.* **66**, 93–104 (2024).
40. Liu, L. et al. Mesenchymal stem cell aggregation-released extracellular vesicles induce CD31+ EMCN+ vessels in skin regeneration and improve diabetic wound healing. *Adv. Healthc. Mater.* **12**, e2300019 (2023).
41. Yang, M. et al. MiR-497∼195 cluster regulates angiogenesis during coupling with osteogenesis by maintaining endothelial Notch and HIF-1α activity. *Nat. Commun.* **8**, 16003 (2017).
42. Chen, X. et al. PIM1/NF-κB/CCL2 blockade enhances anti-PD-1 therapy response by modulating macrophage infiltration and polarization in tumor microenvironment of NSCLC. *Oncogene.* **43**, 2517–2530 (2024).
43. Jin, C. et al. The CCL5/CCR5/SHP2 axis sustains Stat1 phosphorylation and activates NF-κB signaling promoting M1 macrophage polarization and exacerbating chronic prostatic inflammation. *Cell Commun. Signal.* **22**, 584 (2024).
44. Zhuo, C. et al. CXCL1 promotes colon cancer progression through activation of NF-κB/P300 signaling pathway. *Biol. Direct* **17**, 34 (2022).
45. Nie, F. et al. The role of CXCL2-mediated crosstalk between tumor cells and macrophages in Fusobacterium nucleatum-promoted oral squamous cell carcinoma progression. *Cell Death Dis.* **15**, 277 (2024).
46. Jin, W. J. et al. NF-κB signaling regulates cell-autonomous regulation of CXCL10 in breast cancer 4T1 cells. *Exp. Mol. Med.* **49**, e295 (2017).
47. Solis, A. G. et al. Mechanosensation of cyclical force by PIEZO1 is essential for innate immunity. *Nature* **573**, 69–74 (2019).
48. Wang, J. et al. Vascular smooth muscle cell senescence promotes atherosclerosis and features of plaque vulnerability. *Circulation* **132**, 1909–1919 (2015).
49. Lai, A. et al. Mechanosensing by Piezo1 and its implications for physiology and various pathologies. *Biol. Rev. Camb. Philos. Soc.* **97**, 604–614 (2022).
50. Tang, H. et al. Piezo-type mechanosensitive ion channel Component 1 (Piezo1): a promising therapeutic target and its modulators. *J. Med. Chem.* **65**, 6441–6453 (2022).
51. Bryniarska-Kubiak, N. et al. Mechanotransductive receptor Piezo1 as a promising target in the treatment of neurological diseases. *Curr. Neuropharmacol.* **21**, 2030–2035 (2023).
52. Li, Q. & Verma, I. M. NF-κB regulation in the immune system. *Nat. Rev. Immunol.* **2**, 725–734 (2002).
53. Korc, M. RelA: a tale of a stitch in time. *J. Clin. Investig.* **126**, 2799–2801 (2016).
54. Wang, J. et al. RelA/p65 functions to maintain cellular senescence by regulating genomic stability and DNA repair. *EMBO Rep.* **10**, 1272–1278 (2009).
55. Furmanik, M. et al. Reactive oxygen-forming Nox5 links vascular smooth muscle cell phenotypic switching and extracellular vesicle-mediated vascular calcification. *Circ. Res.* **127**, 911–927 (2020).
56. Rodier, F. & Campisi, J. Four faces of cellular senescence. *J. Cell Biol.* **192**, 547–556 (2011).
57. Pan, H. et al. Atherosclerosis is a smooth muscle cell-driven tumor-like disease. *Circulation* **149**, 1885–1898 (2024).
58. Lai, A. et al. Endothelial response to the combined biomechanics of vessel stiffness and shear stress is regulated via Piezo1. *ACS Appl. Mater. Interfaces* **15**, 59103–59116 (2023).
59. Baratchi, S. et al. Piezo1 expression in neutrophils regulates shear-induced NETosis. *Nat Commun* **15**, 7023 (2024).
60. Arenas, G. A. et al. Transcriptional profiling of human endothelial cells unveils PIEZO1 and mechanosensitive gene regulation by prooxidant and inflammatory inputs. *Antioxidants* **12**, 1874 (2023).
61. Ahuja, G. et al. The effects of whole-body vibration therapy on immune and brain functioning: current insights in the underlying cellular and molecular mechanisms. *Front. Neurol.* **15**, 1422152 (2024).
62. Guo, Q. et al. NF-κB in biology and targeted therapy: new insights and translational implications. *Signal Transduct Target Ther.* **9**, 53 (2024).

Acknowledgements

This study was supported financially by grants from the National Natural Science Foundation of China (82204007) and the Guangdong Basic and Applied Basic Research Foundation (2024A1515013049, 2022A1515011357, 2022A1515012412). The funders had no role in the study design, data collection and analysis, and interpretation of the data.

Author contributions

Q.S.C. and H.Y.Y. conceived and supervised the study. Y.S.Z., Z.Q.W. and M.T.X. performed the experiments. Y.S.Z. and Z.Y.C collected, analyzed and interpreted the data. Y.S.Z., Z.S.L., H.M.H and Z.Y.C recruited and collected the human plasma for analysis. Y.S.Z. wrote the manuscript. Q.S.C. and H.Y.Y. revised the manuscript. All authors have read and verified the underlying data and approved the final version of the manuscript.

Competing interests

The authors declare no competing interests.

Additional information

Supplementary information The online version contains supplementary material available at https://doi.org/10.1038/s42003-025-07524-y.

Correspondence and requests for materials should be addressed to Hongyu Yang or Qingsong Chen.

Peer review information *Communications Biology* thanks Sara Baratchi and the other, anonymous, reviewer(s) for their contribution to the peer review of this work. Primary Handling Editors: Ngan F. Huang and Joao Valente. A peer review file is available.